Journal of Applied Polymer Science

Nanocomposites of Ethylene Vinyl Alcohol Copolymer with Thermally Resistant Cellulose Nanowhiskers by Melt Compounding (II): Water Barrier and Mechanical Properties

Marta Martínez-Sanz, Amparo Lopez-Rubio, Jose M. Lagaron
Novel Materials and Nanotechnology Group, IATA, CSIC, Av. Agustín Escardino 7, 46980 Paterna (Valencia), Spain
Correspondence to: J. M. Lagaron (E-mail: lagaron@iata.csic.es)

ABSTRACT: In the present work, the crystallinity and crystalline morphology, thermal stability, water barrier, and mechanical properties of ethylene vinyl alcohol copolymer (EVOH) nanocomposites prepared by melt compounding and incorporating both plant (CNW) and bacterial cellulose nanowhiskers (BCNW) are reported. An improvement in the water barrier performance was observed, that is, 67% permeability drop, only for the microcomposite sample incorporating 2 wt % of bacterial cellulose fibrils. No significant differences in the water-barrier properties of the nanocomposites generated through the two studied preincorporation methods were observed despite the fact that an excellent dispersion was observed in the previous study. On the other hand, direct melt-mixing of the freeze-dried nanofiller with EVOH resulted in increased water permeation. The aggregation of the filler in the latter nanocomposite was also ascribed to the detrimental effect on the mechanical properties. Interestingly, by using the precipitation method, an increase in the elastic modulus and tensile strength of ~36 and 22%, respectively, was observed for a 3 wt % BCNW loading, which was thought to coincide with the percolation threshold. © 2012 Wiley Periodicals, Inc. J. Appl. Polym. Sci. 000: 000–000, 2012

KEYWORDS: biomaterials; cellulose and other wood products; biopolymers and renewable polymers

Received 14 June 2012; accepted 3 August 2012; published online
DOI: 10.1002/app.38432

INTRODUCTION

Ethylene vinyl alcohol copolymers (EVOH) are random semicrystalline materials with excellent gas-barrier properties to oxygen and organic compounds, considerable chemical resistance, and high transparency.[1] An important application of these materials is as barrier layer in multilayer structures to be used in various packaging designs for foodstuffs. The presence of EVOH in the packaging structure is key to food quality and safety, because it reduces the ingress of oxygen and the loss of aroma components during extended packaging shelf-life. However, in high-relative humidity conditions, the EVOH gas barrier and mechanical properties are significantly deteriorated.[2,3] This deterioration is thought to derive from the fact that the inter- and intramolecular hydrogen bonding (so-called self-association) provided by the hydroxyl groups is intercepted by water molecules. This interaction strongly reduces interchain cohesion and mechanical integrity and increments the fractional free volume of the polymer (plasticization effect) for the permeants to travel across polymer packages. Therefore, EVOH is commonly found as an intermediate layer in co-extruded multilayer structures protected by, at least, two layers of hydrophobic materials such as polyolefins.

An alternative for enhancing EVOH water-barrier performance has been the development of EVOH nanocomposites incorporating low amounts of different nanoclays such as modified montmorillonite[4,5] and kaolin[6] by using the melt-compounding technique. The incorporation of microfibrillated cellulose (MFC) into EVOH by the solution-casting technique has also been investigated.[7] In this latter case, a decrease in the water-barrier properties of the films was observed when incorporating MFC. This detrimental effect was ascribed to decreased crystallinity of the matrix and probably also to the hydrophilic character of MFC.

Cellulose nanowhiskers (CNW) have proven to efficiently enhance the barrier properties of polymeric matrixes such as polylactic acid (PLA)[8] and carrageenan[9] when incorporated by means of solution casting. In the case of PLA, improvements of ~82 and 90% in the water and oxygen permeability, respectively, were reported for 3 wt % CNW loadings. For the same CNW loading, a water permeability drop of ~70% was observed in the carrageenan nanocomposites. In both cases, a high-dispersion level of the CNW across the matrix was a crucial factor for obtaining such outstanding improvements on the barrier properties. Unfortunately, achieving such a good

dispersion becomes an issue when using conventional industrial melt-processing techniques. Biopolymer composites of poly(3-hydroxybutyrate-*co*-3-hydroxyvalerate) (PHBV) incorporating CNW were developed by both solution casting and melt compounding.[10] A good dispersion was achieved by means of the first method, whereas the latter one led to CNW's agglomeration despite using polyethylene glycol as compatibilizer. As a result, the melt-processed PHBV/CNW composites exhibited decreased strength, but the glass transition temperature remained unmodified. It has also been attempted to prepare PLA nanocomposites reinforced with CNW by pumping a suspension of CNW in DMAc/LiCl into the polymer melt during the extrusion process.[11] In this case, aggregation and thermal degradation took place to a certain extent, and, even when PVA was used as compatibilizer, it was not possible to attain a morphology of well-dispersed CNW.[12]

In the first part of this study, the use of the electrospinning technique, as well as a solution-precipitation method, was proposed as innovative methods for the incorporation of homogeneously distributed bacterial and plant CNW into an EVOH matrix by means of melt compounding. The electrospinning technique has been previously applied for the incorporation of CNW in polymeric matrixes such as polystyrene,[13] poly(vinyl alcohol),[14] or poly(methyl methacrylate),[15] and the method for generating electrospun EVOH-BCNW hybrid fibers has been optimized in a previous work.[16] The use of these electrospun fibers as a way of enhancing the dispersion of BCNW in EVOH by melt compounding was also proposed, and this method was shown to give rise to a better dispersion of the nanofiller when compared with the direct melt-mixing of freeze-dried BCNW with the polymeric matrix.[17] Nevertheless, due to the acidic character of the BCNW, their thermal stability was not high enough to stand the temperatures applied during melt processing, and thermal degradation took place to a certain extent.

In the previous part of this work,[18] BCNW with improved thermal stability were also incorporated into electrospun EVOH fibers, and this technique was proposed as a way of enhancing the dispersion of the nanofiller in the nanocomposites subsequently obtained by melt compounding. The effects of the incorporation method, the nanofiller loading, and cellulose source on the morphology and thermal properties of the developed nanocomposites were investigated. In the current work, the crystallinity, thermal stability, water-barrier properties, and mechanical properties of the nanocomposite materials are evaluated and related to the previous morphological observations.

MATERIALS AND METHODS

Materials

Ethylene-vinyl alcohol copolymer grade (Soarnol) EVOH32 (containing 32 mol % of ethylene) was supplied by The Nippon Synthetic Chemical Industry Co. (NIPPON GOHSEI) (Japan). Sulfuric acid 96% and 2-propanol were purchased from Panreac (Barcelona, Spain).

Bacterial cellulose (BC) mats were obtained following a procedure similar to the one described in a previous work[16] and were supplied by BioInicia S.L. (Valencia, Spain).

For the production of plant CNW, a purified cellulose microfiber grade from CreaFill Fibers Corp. (US), having an average fiber length of 60 μm and an average fiber width of 20 μm, was used as a raw material. According to the manufacturer's specifications, these fibers had an α-cellulose content in excess of 99.5%.

Bacterial cellulose nanowhiskers (BCNW) and plant CNW were prepared as described in the previous part of this work,[18] and detailed procedures can be found elsewhere.[8,16]

Preparation of Films

Nanocomposite EVOH films were prepared using three different methods: the traditional method of melt-mixing the matrix directly with the freeze-dried nanofiller, and two novel methods of incorporating CNW in the EVOH matrix, previous to the melt-compounding stage, just as explained in the previous part of this work.[18]

X-Ray Diffraction

X-ray diffraction was carried out on a D5005 Bruker diffractometer. The instrument was equipped with a Cu tube and a secondary monochromator. The configuration of the equipment was θ–2θ, and the samples were examined over the angular range of 5°–45° with a step size of 0.02° and a count time of 4 s per point.

Peak fitting was carried out using Igor software package (Wavemetrics, Lake Oswego, OR). A Lorentzian function was used to fit the experimental diffraction profiles obtained. For the fitting procedure, the reflections considered were as follows: (i) three at 11°, 20.2°, and 22° 2θ (corresponding to the 100, 110, and 200 crystal planes, respectively) assigned to the orthorhombic lattice of EVOH[3] or four reflections at 10.8°, 19.8°, 20.2°, and 22.5° 2θ (corresponding to the 100, 110, $1\bar{1}0$, and 200 crystal planes, respectively) assigned to the monoclinic lattice of EVOH[3]; (ii) two at 14.8° and 16.4° (corresponding to the 101 and $10\bar{1}$ crystal planes, respectively) assigned to the cellulose I allomorph, for these samples in which the cellulose contribution could be detected; and (iii) the amorphous halo centered at ~20° 2θ. The crystallinity index CI (XD) was determined by the method reported by Wang et al.[19]:

$$\mathrm{CI(XD)} = \frac{\sum A_{\mathrm{Crystal}}}{A_{\mathrm{Total}}} \times 100$$

where A_{Total} is the sum of the areas under all the diffraction peaks and $\Sigma A_{\mathrm{Crystal}}$ is the sum of the areas corresponding to crystalline peaks.

Thermogravimetric Analysis

Thermogravimetric curves were recorded with a TA Instruments model Q500 TGA. The samples (~20 mg) were heated from 50 to 600°C with a heating rate of 10°C/min under nitrogen atmosphere. Derivative TG curves express the weight loss rate as a function of temperature.

Water Permeability

Direct permeability to water vapor was determined from the slope of the weight loss versus time curves at 24°C. The films were sandwiched between the aluminum top (open O-ring) and bottom (deposit for the permeant) parts of a specifically designed permeability cell with screws. A Viton rubber O-ring was placed between the film and the bottom part of the cell to enhance sealability. These permeability cells containing water as the permeant

were then placed inside a desiccator at 0% RH, and the solvent weight loss through a film area of 0.001 m^2 was monitored and plotted as a function of time. The samples were preconditioned at the testing conditions for 24 h, and to estimate the permeability values of the films, only the linear part of the weight loss data was used to ensure sample steady-state conditions. Cells with aluminum films were used as control samples to estimate solvent loss through the sealing. The lower limit of WVP detection of the permeation cells was of $\sim 0.008 \cdot 10^{-15}$ kgm/s m^2 Pa based on the weight loss measurements of the aluminum films. Solvent permeation rates were estimated from the steady-state permeation slopes. Water vapor weight loss was calculated as the total cell weight loss minus the loss through the sealing. The tests were done in duplicate.

Density Measurements

The density of EVOH and nanocomposite films was determined by the density-gradient technique using a density column as described by the ASTM D1505 standard. Briefly, a density gradient column (CEAST) was filled in with two different solvents (toluene and dichloromethane) in order to create a gradient range suitable to determine the density of the EVOH specimens. Standard glass floats were dropped into the column solution, and, once they stabilized, a calibration curve was built by relating their position with their known density values. Subsequently, EVOH specimens were added to the column, and their densities were calculated by extrapolating their position into the calibration curve.

From the density values obtained, together with the overall crystallinity index (X_c), the crystallinity of BCNW, BC, or CNW as determined by XRD, the crystalline density of EVOH calculated from the lattice crystal parameters from the XRD patterns, and the crystalline density of cellulose ($\rho_{c\ \text{cellulose}} = 1.59$ g/cm^3),[20] the density of the amorphous phase (ρ_a) was determined.

Water Uptake

The water uptake was estimated during sorption experiments at 24°C and 100% RH by means of weight gain using an analytical balance Voyager® V11140. Thus, at saturation conditions, no changes in successive weight uptake were observed during the measurements of the specimens.

Solubility (S), required to estimate the diffusion coefficient of water (D) through the films, was estimated from the water uptake at equilibrium, the density of the materials, and the water vapor partial pressure at 24°C.

Mechanical Properties

Tensile tests were carried out at ambient conditions typically at 24°C and 50% RH on an Instron 4400 Universal Tester. Preconditioned dumb-bell-shaped specimens with initial gauge length of 25 and 5 mm in width were die-stamped from the films in the machine direction according to the ASTM D638. A fixed crosshead rate of 10 mm/min was used in all cases, and results were taken as the average of four tests.

Statistical Analysis

One-way analysis of the variance (ANOVA) was performed using XLSTAT-Pro (Win) 7.5.3 (Addinsoft, NY) software package. Comparisons between samples were evaluated using the Tukey's test.

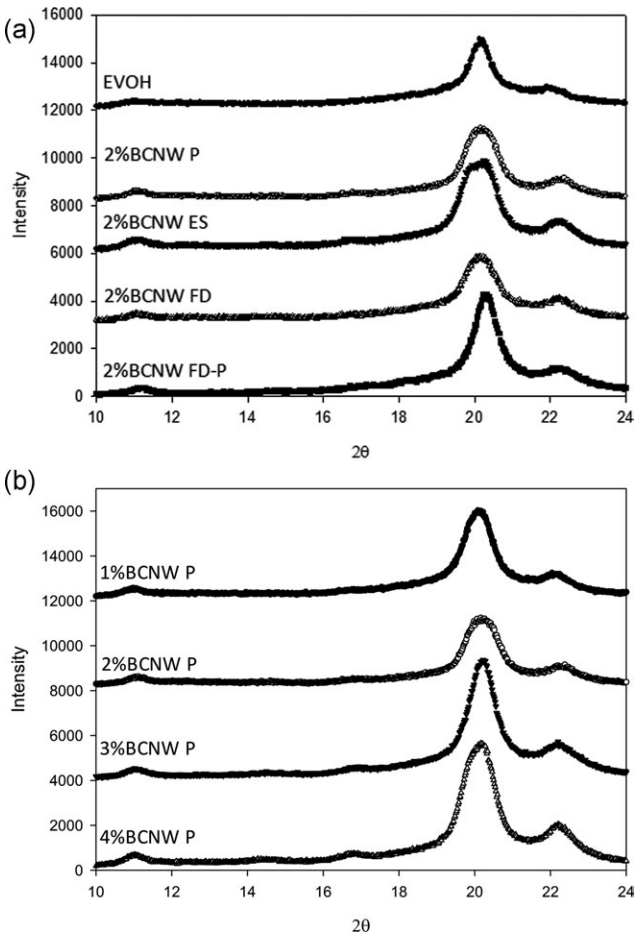

Figure 1. X-ray diffraction patterns of neat EVOH film and films containing 2 wt % BCNW (a) and films containing different concentrations of BCNW incorporated by the precipitation method (b).

RESULTS AND DISCUSSION

Nanocomposite EVOH Films Reinforced with BCNW

Effect of BC Addition on the Crystallinity of the Nanocomposite Films. In the previous part of this study, DSC analyses showed that the incorporation of CNW slightly reduced the crystallinity of EVOH, especially when aggregation took place or for high nanofiller loadings.[18] However, the nanofiller possessed a high crystallinity index and, thus, the effect on the overall crystallinity of the nanocomposite material was expected to depend on the nanowhiskers loading and degree of dispersion. Figure 1(a) shows the XRD patterns of the neat EVOH film and of the nanocomposite films with 2 wt % BCNW through the different incorporation methods. The contribution of cellulose was observed in all the samples as an increase in the intensity of the peak located at $2\theta \sim 20°$. This peak corresponds to the 002 crystallographic plane of cellulose I,[21] which is usually observed at 22.5° 2θ and, in this case, it was overlapped with the 110 reflection of orthorhombic EVOH. Furthermore, for loadings greater than 2 wt %, the less-intense reflections at 14.8° and 16.4°, corresponding to the 101 and $10\bar{1}$ crystal planes from cellulose I, respectively, could also be identified in the diffraction patterns [cf. Figure 1(b)]. It is also interesting to note that the incorporation of BCNW led to a certain modification of the EVOH

Applied Polymer SCIENCE

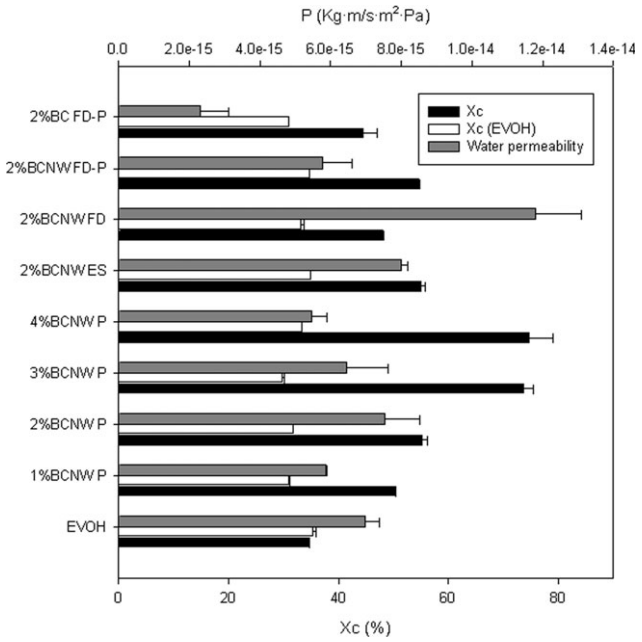

Figure 2. Crystallinity index determined from the XRD patterns (X_c) and crystallinity index of the EVOH matrix obtained by DSC analyses[18] [X_c (EVOH)] (lower axis) and water permeability (upper axis).

crystal unit cell. As observed in Figure 1(a), while the neat EVOH film displayed the diffraction peaks characteristic from the orthorhombic crystal lattice, probably due to the rapid cooling rate during the film preparation method,[3] the diffractograms from the nanocomposite films showed a broadening of the 110 reflection at ~20° 2θ pointing out that an intermediate state between the orthorhombic lattice and the more thermodynamically stable monoclinic polymorph was developed in these samples. These results indicate that even though addition of BCNW somehow hindered crystallization, as confirmed in the previous part of this work by DSC,[18] the crystals formed were thermodynamically more stable (as it will be confirmed later on by the crystal density measurements). This apparent counterintuitive behavior seems to be caused by the whiskers, which it is hypothesized to impede the growth of crystals and, perhaps, also reduce the likelihood of incorporating defects in the crystallinity.

The crystallinity values calculated from these diffraction patterns, as well as the ones obtained for the EVOH matrix by the DSC analyses carried out in the first part of this study,[18] are shown in Figure 2 for comparison purposes. It is interesting to see that there was a good agreement between the pure EVOH crystallinity index previously obtained from DSC experiments (35.3 ± 0.7) and the one calculated from the XRD patterns of the EVOH film (34.65 ± 0.01). From Figure 2, it is observed that addition of the highly crystalline BCNW gave rise to an increase in the overall crystallinity index of the material, which mainly depended on the BCNW's concentration, but also on the degree of filler dispersion, which was related to the incorporation method. The following crystallinity indexes were estimated for nanocomposites produced by the precipitation method: 50.4 ± 0.2, 55.1 ± 4.5, 74.6 ± 1.1, and 75.7 ± 1.7 for 1, 2, 3, and 4 wt % BCNW loading, respectively. As observed, the crystallinity of the material increased with higher nanofiller loadings, although this increase was more pronounced for concentrations greater than 2 wt %.

On the other hand, the sample 2% BCNW FD displayed significantly lower crystallinity (50.0 ± 0.5) than the other samples with the same loading level but prepared using the novel electrospinning and precipitation methods (55.1 ± 0.2, 55.1 ± 4.5, and 54.6 ± 1.6, for 2% BCNW ES, 2% BCNW P, and 2% BCNW FD-P, respectively). Therefore, in agreement with the morphological study carried out in the previous part of this work, it seems that the agglomeration of BCNW led to lower crystallinity as a result of the detrimental effect of agglomerated nanofiller on the EVOH crystallinity. The nanocomposite containing the BC microfibers also displayed significantly lower overall crystallinity, due to the combination of the lower EVOH matrix crystallinity and to the fact that this filler had an intrinsic lower crystallinity as it did not undergo the hydrolysis treatment.

Water Permeability of the EVOH Nanocomposite Films Containing BC. Regarding the water-barrier properties, water permeability and sorption experiments were carried out, and the results, together with the estimated diffusion coefficient, are summarized in Table I. The general trend when incorporating BCNW into the EVOH films was a slight decrease in the water permeability (P) of the nanocomposites, although for most of the samples, there was not a statistically significant effect, and there were some exceptions as discussed later on. For most of the nanocomposites, the solubility (directly related to the water uptake) decreased with the incorporation of highly crystalline BCNW, because the amorphous fraction of material that was available for water sorption was reduced.

Interestingly, the incorporation of BCNW led to a decrease on the amorphous density of the material. This decrease was more obvious at higher nanofiller loadings, and it may be related to the disruption of the strong polymer inter- and intrachain self-association by the dispersed cellulose filler. Thus, the dispersed cellulose interacted with the hydroxyl groups of the polymer, increasing the available free volume, which is in turn filled in by the whiskers.

From the results compiled in Table I, it clearly seems that the method of nanofiller incorporation had an important effect on the water vapor permeability of the materials. When the traditional method was used, that is, directly melt-mixing the freeze-dried nanowhiskers with EVOH pellets (cf. 2% BCNW FD), an increase in the permeability of ~69% was observed, being this negative effect mainly explained by increased water diffusion through the film as a consequence of the potential preferential paths generated in areas where the filler agglomerated and by importantly by plasticization of these agglomerates. The increase in water permeability was largely avoided by improving the dispersion of the nanofiller via the novel incorporation methods. However, while remarkable reductions in water permeability of ~67% were detected for the 2% BC FD-P sample, the water permeability in the samples incorporating dispersed BCNW for this specific loading, that is, 2% BCNW ES, 2% BCNW P, and

Table I. Water Permeability, Water Uptake, Diffusion Coefficient, Crystalline (ρ_C), and Amorphous Density (ρ_a) for EVOH32, and EVOH Composites Incorporating BC and BCNW

	P (kg m/s m^2 Pa)	Water uptake 100% RH (%)	D (m^2/s)	ρ_C (g/cm^3)	ρ_a (g/cm^3)
EVOH32	$^{b}6.99 \pm 0.39\ e^{-15}$	$^{c,d}9.25 \pm 0.20$	$^{a,b,c}1.88 \pm 0.04\ e^{-13}$	1.48	1.09
1% BCNW P	$^{b}5.88 \pm 0.01\ e^{-15}$	$^{a,b,c}7.93 \pm 0.33$	$^{a,b,c}1.86 \pm 0.08\ e^{-13}$	1.48	0.99
2% BCNW P	$^{b}7.55 \pm 0.97\ e^{-15}$	$^{b,c,d}8.62 \pm 0.43$	$^{b,c}2.19 \pm 0.00\ e^{-13}$	1.49	0.96
3% BCNW P	$^{b}6.45 \pm 1.19\ e^{-15}$	$^{a,b,c}7.81 \pm 0.28$	$^{a,b,c}2.06 \pm 0.07\ e^{-13}$	1.50	0.74
4% BCNW P	$^{b}5.45 \pm 0.46\ e^{-15}$	$^{a,b}7.05 \pm 0.36$	$^{a,b,c}1.92 \pm 0.97\ e^{-13}$	1.49	0.77
2% BCNW ES	$^{b}7.99 \pm 0.18\ e^{-15}$	$^{a}6.99 \pm 0.94$	$^{c,d}2.86 \pm 0.39\ e^{-13}$	1.51	0.95
2% BCNW FD	$^{c}11.8 \pm 0.13\ e^{-15}$	$^{a,b}7.12 \pm 0.23$	$^{d}4.20 \pm 0.14\ e^{-13}$	1.49	0.99
2% BCNW FD-P	$^{b}5.78 \pm 0.84\ e^{-15}$	$^{d}10.01 \pm 0.01$	$^{a,b}1.38 \pm 0.04\ e^{-13}$	1.50	0.95
2% BC FD-P	$^{a}2.32 \pm 0.79\ e^{-15}$	$^{a,b,c}7.75 \pm 0.16$	$^{a}0.77 \pm 0.02\ e^{-13}$	1.50	1.02

The a, b, c, and d letters correspond to the ANOVA statistical analysis and Tukey test of the data that indicate that with a 95% confidence level, and the values are significantly different.

2% BCNW FD-P, was not significantly modified. Therefore, aside from the degree of dispersion of the filler and the crystallinity of the samples, it seems that more factors come into play when it comes to the barrier performance of the nanocomposite materials. A possible explanation for these results comes again from the interactions developed between the dispersed BCNW and the EVOH matrix, which resulted in a decrease in the amorphous density, which, at the same time, had a direct influence on the water diffusion through the films. As a consequence, the water permeability results are a combination of all the above-mentioned factors, that is, the advantages of increased crystallinity and dispersion together with the disadvantages of the increased free volume as a consequence of the inter- and intrapolymer disruptions caused by the presence of BCNW. Furthermore, the hydrophilic character of the filler and the morphology of the same should also be taken into account for explaining the water-barrier properties. Therefore, the fact that BC fibers were longer, because they had not been digested by sulfuric acid, could also explain the improved permeability observed for this specific material. In a similar way, lower permeability has been reported for MFC films when compared with films containing CNW[22] due to entanglements of longer fibers, which lead to increased tortuosity of the diffusion pathway.

Although no significant differences were detected for the permeability of the different BCNW concentrations incorporated through the precipitation method, a maximum permeability drop of 22% was observed for the 4 wt % loading. The usual behavior that has been previously reported for PHBV and PCL matrixes incorporating cellulose microfibers consists of decreased water barrier properties when increasing the nanofiller loading over 2 wt %, because higher nanofiller loadings led to agglomeration.[23] However, this was not the case for the nanocomposites in the present study, because morphological observations did not show significant agglomeration of BCNW for the loadings investigated.[18] It seems that the crystallinity increase observed for loadings higher than 3 wt % (cf. Figure 2) was responsible for a decrease in the water sorption high enough to counteract the effect of the reduction in the amorphous density of the material.

To better assess the barrier performance, experimental data were compared to the results obtained when applying a theoretical model. Maxwell[24] developed a model to describe the conductivity of a two-phase system in which permeable spheres (P_d) are dispersed in a continuous permeable matrix (P_m). Fricke[25] extended Maxwell's model to describe the conductivity of a two-phase system in which ellipsoids with permeability P_d are dispersed in a more permeable continuous matrix. According to this model, the permeability of the composite system (being Φ_2 the volume fraction of the dispersed phase) can be expressed as follows[26]:

$$P = (P_m + P_d F)/(1 + F) \quad (1)$$

where P is the permeability of the composite, P_m is the permeability of the matrix and

$$F = [\phi_2/1 - \phi_2][1/(1 + (1 - M(P_d/P_m - 1))]$$
$$M = \cos\theta/\sin^3[\theta - 1/2\ \sin 2\theta]$$
$$\cos\theta = W/L$$

W and L are the dimensions of the axis of the ellipsoid parallel and perpendicular, respectively, to the direction of transport and θ is in radians. The following parameters were used in eq. (1): $P_d \approx 0$, $P_m = 100$, and L/W of 5, 10, 30, and 70.

To calculate the volume fraction ϕ the following expression was applied[27]:

$$\varphi = \frac{w_r/\rho_r}{w_r/\rho_r + (1 - w_r)/\rho_m}$$

where w_r refers to the weight fraction of the reinforcement, and ρ_r and ρ_m refer to the density of the reinforcement and the matrix, respectively. In this case, we considered $\rho_{EVOH} = 1.2$ g/cm[31] and $\rho_{cellulose} = 1.6$ g/cm^3.[25]

Figure 3 plots the experimental relative permeability values and the modeling results. It was previously observed by TEM that BCNW presented an aspect ratio of ~30.[18] As observed in Figure 3, if considering L/W as 30, the experimental values were above the predicted ones. To estimate the barrier efficiency of the

Applied Polymer SCIENCE

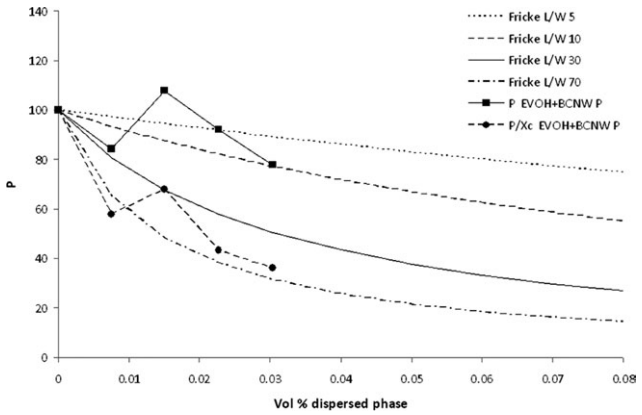

Figure 3. Permeability modeling versus volume percent of a dispersed phase with different aspect ratios *L*/*W* and the normalized experimental permeability values.

nanofiller and separating the effect of the increase in the crystallinity of the material, the permeability values were corrected by dividing them by the crystallinity of the material estimated by XRD.[28] When plotting the permeability values corrected by the crystallinity, it is observed that values were better fitted to the model when considering *L*/*W* as 70. Thus, it seems that the blocking capacity of the highly crystalline BCNW is underestimated by the theoretical model. Again, it seems that the decrease in the amorphous density of the material was responsible for the increase in the permeability for loadings up to 2 wt %, whereas the high crystallinity attained for higher loadings was able to counteract this negative effect, leading to a maximum permeability decrease for the 4 wt % BCNW nanocomposite.

Mechanical Properties of the Different EVOH/BC Nanocomposite Films. Table II gathers the mechanical properties of neat EVOH and the nanocomposites thereof. From the results, it can be concluded that, in general, with the addition of BCNW, the materials become more rigid and brittle.

For a 2 wt % BCNW loading, a significant increase of 80% and 18% in the tensile modulus of the material was observed for the 2% BCNW FD-P and 2% BCNW FD samples, respectively, suggesting that when the filler was incorporated as a freeze-dried product, the filler–filler interactions were promoted, and thus, a strong nanofiller network was responsible for the stiffening of the nanocomposites.

When comparing amongst the different composite samples containing 2 wt % of filler, although a significant reduction in the elongation at break was observed for all of them, the greatest reduction was seen for the 2% BCNW FD (94% drop), 2% BCNW FD-P (94% drop), and 2% BC FD-P (92% drop) samples. It is known that the addition of reinforcing agents in polymeric materials results in a reduction of the elongation at break, because they act as stress-concentrating components. However, previous works found out that when strong interactions, such as hydrogen bonding, take place between the matrix and the filler, the stress-concentration effect is prevented to a certain extent.[29] These results suggest a lower interfacial interaction effect and/or poorer dispersion of the nanofiller when handling it in the form of freeze-dried material. On the other hand, and in agreement with morphology observations[18] and water permeability results, it seems that the incorporation of the BCNW within electrospun fibers or through precipitation from a hydrated nanofiller may be led to improved interactions with the polymeric matrix and, hence, to a less brittle behavior (cf. elongation at break results in Table II).

Regarding the BCNW concentration in the samples obtained through the precipitation method, it was observed that a maximum increase of 36% and 22% in the Young's modulus and tensile strength, respectively, was produced for a 3 wt % loading. Moreover, this concentration did not lead to a significant decrease in the elongation at break, while remarkable reductions were observed for the 2 and 4 wt % loadings. It seems that 3 wt % BCNW was the optimum concentration in which both the filler–filler and the matrix–filler interactions were favored.

It is worth to mention that the incorporation of BCNW led to a decrease in the energy absorbed by the material at break (i.e., toughness), but in the case of the 2% BCNW ES, 3% BCNW P, and 1% BCNW P, this drop was minimized. It is known that the mobility of the nanofiller within the polymeric matrix and further nanoparticle alignment under applied tensile stress is essential for energy dissipation and, thus, enhanced toughness.[30]

Table II. Young's Modulus, Tensile Strength, and Elongation at Break for EVOH32 and EVOH Composites Incorporating BC and BCNW

	E (GPa)	Tensile strength (MPa)	ε_b (%)	Toughness (J)
EVOH	^{a}1.37 ± 0.18	^{a,b}51.99 ± 4.96	^{c}93.35 ± 56.52	^{d}0.36 ± 0.14
1% BCNW P	^{a}1.34 ± 0.11	^{a,b}49.75 ± 2.59	^{b,c}66.13 ± 46.34	^{b,c}0.11 ± 0.03
2% BCNW P	^{a,b}1.51 ± 0.14	^{a,b,c}53.06 ± 3.23	^{a}11.25 ± 5.72	^{a,b}0.04 ± 0.00
3% BCNW P	^{c}1.87 ± 0.06	^{c,d}63.56 ± 1.30	^{a,b}34.78 ± 21.40	^{b,c}0.14 ± 0.08
4% BCNW P	^{a,b}1.54 ± 0.11	^{a,b,c}55.46 ± 3.83	^{a}13.48 ± 10.90	^{a,b,c}0.07 ± 0.03
2% BCNW ES	^{a,b}1.45 ± 0.07	^{a}46.81 ± 0.74	^{a,b}30.85 ± 16.18	^{c}0.16 ± 0.05
2% BCNW FD	^{b,c}1.62 ± 0.22	^{b,c}56.29 ± 10.60	^{a}5.48 ± 3.31	^{a}0.02 ± 0.02
2% BCNW FD-P	^{d}2.46 ± 0.19	^{d}74.46 ± 4.84	^{a}5.53 ± 1.17	^{a,b}0.02 ± 0.00
2% BC FD-P	^{a,b,c}1.63 ± 0.11	^{a,b}50.65 ± 2.48	^{a}7.97 ± 1.67	^{a,b,c}0.04 ± 0.03

The a, b, c, and d letters correspond to the ANOVA statistical analysis and Tukey test of the data that indicate that with a 95% confidence level, and the values are significantly different.

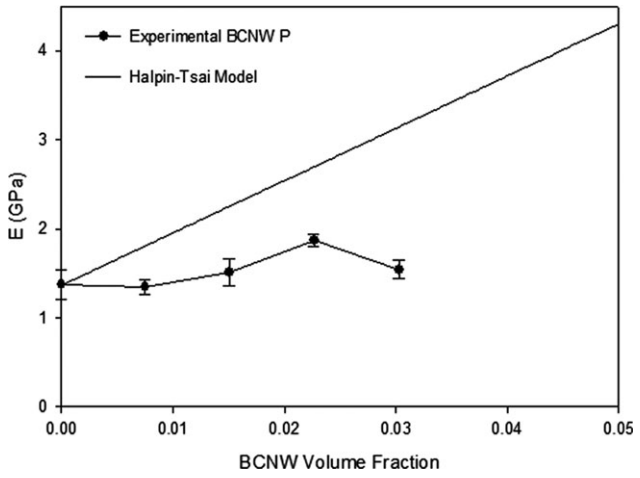

Figure 4. Experimentally measured Young's modulus for EVOH-BCNW P nanocomposites compared to theoretical predictions by Halpin–Tsai.

Hence, it appears that a greater dispersion and mobility of the nanowhiskers was achieved in the former nanocomposites.

Previous studies have reported that the addition of cellulose whiskers resulted in a decrease in the mechanical properties due to poor interfacial adhesion between a hydrophobic matrix and the highly hydrophilic CNW.[8,31] Nevertheless, it has also been reported that in addition to the filler–matrix adhesion, the filler–filler interactions are important for the reinforcing capacity of CNW.[11,31] Achieving the so-called percolation threshold, where the nanowhiskers are strongly interconnected by a 3D network, has been claimed as a crucial condition to obtain strong mechanical reinforcement. By using the following equation, the percolation threshold (υ_{RC}) can be easily estimated on the bases of the aspect ratio[11]:

$$\upsilon_{Rc=\frac{0.7}{L/d}}$$

In the above equation, L/D is the aspect ratio. For the nanocomposites incorporating BCNW, with an experimental aspect ratio of ~32, the percolation threshold should lay around 2 vol % of BCNW. Indeed, as observed in Figure 4, a loading of 2.3 vol % (corresponding to a 3 wt %) gave rise to the optimum in the mechanical properties attained by the addition of BCNW.

Modeling of the mechanical properties using the following Halpin–Tsai equation was also carried out in order to determine the theoretical expectations[32]:

$$E = \frac{E_m(\xi\eta\phi)}{1-\eta\phi}, \eta = \frac{E_r/E_m - 1}{E_r/E_m - \xi} \quad (2)$$

where E_m and E_r refer to the Young's modulus of the matrix and the reinforcement, respectively, ϕ is the volume fraction, and ξ is calculated from the following expression:

$$\xi = \frac{2.\text{Length}}{\text{Thickness}}$$

The following data were used in the calculations: $E_{\text{EVOH}} = 1.4$ GPa, $E_{\text{cellulose}} = 167.5$ GPa.[33] The BCNW dimensions, which were determined in the first part of this work,[18] were 570 × 18 nm.

Figure 4 shows the comparison between the theoretical and experimental results for the Young's modulus. The theoretical calculations were based on fully dispersed systems where the filler was aligned in the longitudinal direction and had perfect interfacial adhesion to the matrix. As observed, the experimental results were clearly below the theoretical ones. In our case, the interfacial adhesion between the matrix and the filler was relatively good, as deduced from the morphological examination of the samples,[18] and, thus, the results may be caused by the fact that processing by melt compounding was detrimental for the cementation of the CNW percolation network. It has been previously reported that the high-polymer melt viscosity that occurs during extrusion limits the random movement and, consequently, hinders the interconnection between CNW. As a result, the percolating structure is not easily formed, and the reinforcing efficiency is lower than for nanocomposites obtained by solvent casting.[34]

It is worth drawing attention to the remarkable mechanical properties of the 3% BCNW P film. The increase in the elastic modulus and tensile strength as a result of the BCNW incorporation indicate that this material was quite stiff and strong, and yet it was relatively ductile if compared to the other nanocomposites.

Thermal Stability of the Different EVOH/BC Nanocomposite Films. Finally, the thermal stability of the nanocomposite materials was evaluated through TGA. As determined in the previous stage of this study,[18] the incorporated BCNW showed a thermal stability, which was improved with respect to the previous results,[16] but still, comparatively lower than that of the polymeric matrix. Table III summarizes the parameters determined from the TGA curves. As it can be seen, incorporation of BCNW did not have a great effect on the thermostability of the copolymer. For the samples containing 2 wt % BCNW, the one incorporating freeze-dried nanowhiskers presented the lowest onset degradation temperature and the widest degradation profile, which was probably caused by the lower interaction of the agglomerated filler with the matrix, which resulted in slightly decreased thermal stability of the nanocomposite. But even in that case, all the nanocomposites were thermally stable in the

Table III. TGA Maximum of the Weight Loss First Derivate (T_D) and the Corresponding Peak Onset And Endset Values for the EVOH-Based Nanocomposites

	Onset T (°C)	T_D (°C)	Endset T (°C)
EVOH	268.9	398.7	483.6
1% BCNW P	251.7	393.7	481.1
2% BCNW P	274.8	398.8	481.8
3% BCNW P	286.7	395.2	477.2
4% BCNW P	291.4	395.4	476.5
2% BCNW ES	278.4	395.2	483.6
2% BCNW FD	265.4	395.6	480.1
2% BCNW FD-P	271.9	394.9	479.7
2% BC FD-P	263.6	394.8	480.8

Applied Polymer SCIENCE

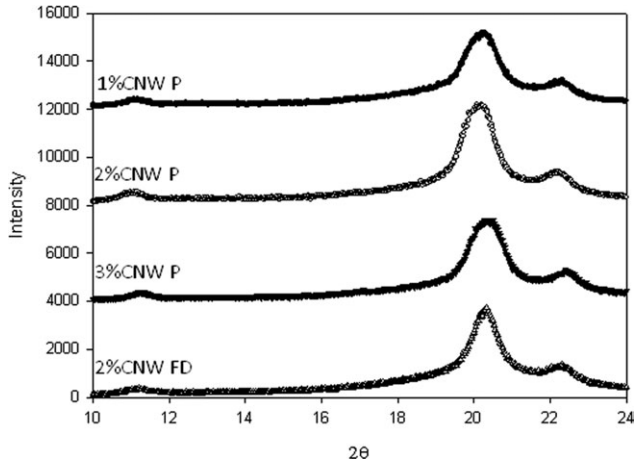

Figure 5. X-ray diffraction patterns of films containing CNW incorporated by the precipitation method and freeze-dried.

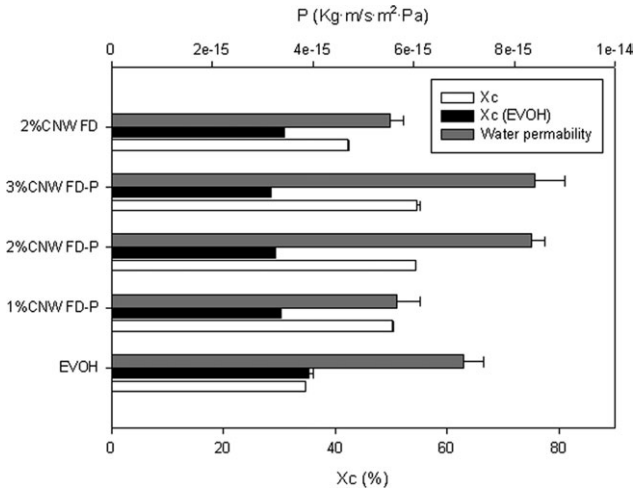

Figure 6. Crystallinity index determined from the XRD patterns (X_c) and crystallinity index of the EVOH matrix obtained by DSC analyses [X_c (EVOH)] (lower axis) and water permeability (upper axis).

temperature range in which EVOH is typically processed, that is, below 185°C.

Nanocomposite EVOH Films Reinforced with Plant CNW

Effect of Plant CNW Addition on the Crystallinity of the Nanocomposite Films. In the first part of this work, it was observed that the crystallinity of plant-derived CNW was lower than that of BCNW.[18] Therefore, a lower increase in the overall crystallinity of films incorporating CNW would be expected when compared with the crystallinity of the films containing BCNW. Figure 5 shows the diffraction patterns of the nanocomposites incorporating CNW. In this case, it was not possible to differentiate the contribution of cellulose apart from the increase in the peak at $2\theta \sim 20°$, which overlapped with the EVOH contribution. As seen in Figure 6, the overall crystallinity of the nanocomposites increased when raising the nanofiller loading. When comparing the incorporation method, and probably due to the greater agglomeration taking place when directly melt-mixing freeze-dried CNW, the crystallinity increase was less pronounced in this specific case.

As expected, the crystallinity increase with CNW was lower than that observed for composites containing BCNW, especially for loadings higher than 2 wt %.

Water Permeability of the EVOH Nanocomposite Films Containing Plant CNW. Table IV gathers the water barrier properties of the nanocomposite EVOH films incorporating CNW as well as the crystalline and amorphous density. Just as observed with the addition of BCNW, the density of the amorphous polymer regions decreased when incorporating CNW. For low loadings, a slight decrease in the water permeability was produced, but concentrations greater than 1 wt % led to an increase in the water permeability with respect to that of neat EVOH. This was a result of an increase in the diffusion coefficient, which was high enough to counteract the reduction in the water solubility. In this case, the incorporation of freeze-dried CNW was beneficial if compared to the pre-incorporation using the precipitation method, because the latter produced a slight permeability increase. This effect might be mainly caused by a greater reduction in the diffusion coefficient for the freeze-dried CNW, suggesting that, even though agglomeration took place to a certain extent, the resulting morphology seemed to be more favorable for blocking the water diffusion. Nevertheless, the incorporation of CNW did not produce a statistically significant effect on the permeability when compared with that of neat EVOH.

As observed in Figure 7, for 1 wt % CNW, the permeability drop was higher than expected according to the theoretical model considering an aspect ratio of ~12, which corresponded to the aspect ratio previously determined for CNW.[18] When further increasing the concentration of CNW, the experimental

Table IV. Water Permeability, Water Uptake, Diffusion Coefficient, Crystalline (ρ_C), and Amorphous Density (ρ_a) for EVOH32 and EVOH Composites Incorporating CNW

	P (kg m/s m^2 Pa)	Water uptake 100% RH (%)	D (m^2/s)	ρ_C (g/cm^3)	ρ_a (g/cm^3)
EVOH	$^{a,b}6.99 \pm 0.39\ e^{-15}$	$^{a}9.25 \pm 0.20$	$^{b}1.88 \pm 0.04\ e^{-13}$	1.48	1.09
1% CNW FD-P	$^{b}5.67 \pm 0.46\ e^{-15}$	$^{a,b}8.90 \pm 0.50$	$^{a}1.59 \pm 0.09\ e^{-13}$	1.50	0.99
2% CNW FD-P	$^{a}8.34 \pm 0.27\ e^{-15}$	$^{b}7.97 \pm 0.05$	$^{b}1.91 \pm 0.01\ e^{-13}$	1.49	0.97
3% CNW FD-P	$^{a}8.40 \pm 0.59\ e^{-15}$	$^{a,b}8.81 \pm 0.47$	$^{c}2.38 \pm 0.13\ e^{-13}$	1.52	1.04
2% CNW FD	$^{b}5.53 \pm 0.27\ e^{-15}$	$^{a,b}8.44 \pm 0.07$	$^{a,b}1.65 \pm 0.01\ e^{-13}$	1.51	0.97

The a, b, and c letters correspond to the ANOVA statistical analysis and Tukey test of the data that indicate that with a 95% confidence level, and the values are significantly different.

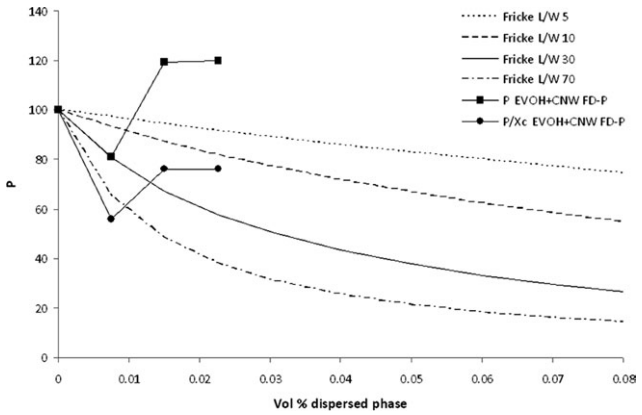

Figure 7. Permeability modeling versus volume percent of a dispersed phase with different aspect ratios *L*/*W* and the normalized experimental permeability values.

values increased showing a completely different behavior from the model predictions. This discrepancy between the experimental data and the model might be due to a significant agglomeration of the nanofiller when increasing the loading above 1 wt %. Indeed, in the first part of this work, morphological studies pointed out the fact that the degree of CNW's agglomeration was considerably increased with the CNW's loading. In addition, it was determined that higher degrees of dispersion were achieved with BCNW than with CNW probably as a consequence of the freeze-drying process applied to the latter ones. This was also manifested in the fact that films incorporating CNW through the precipitation method were more permeable than those containing BCNW mainly due to reduced diffusion when incorporating BCNW. On the contrary, freeze-dried CNW gave rise to lower permeability values when compared with the nanocomposite film incorporating freeze-dried BCNW. The morphology of CNW, which were shorter than BCNW, seemed to favor the blocking capacity when the nanofillers were considerably agglomerated.

Mechanical Properties of the Different EVOH Nanocomposite Films Containing Plant CNW. Mechanical properties of CNW nanocomposites are summarized in Table V. From these results, it can be deduced that the incorporation of CNW did not lead to remarkable improvements on the mechanical properties of the EVOH films. In general, greater tensile modulus, tensile strength, and decreased elongation at break were observed when increasing the CNW loading. An increase of 3, 10.2, and 10.2% in the elastic modulus was observed for the nanocomposites containing 1, 2, and 3 wt % CNW, respectively. For the same samples, a decrease of 1.6% and increases of 0.7 and 7.8% were produced in the tensile strength. Therefore, the materials became more rigid and stronger with the incorporation of CNW through the precipitation method. At the same time, the ductility of the composites was gradually diminished, first increasing a 5.3% for the 1 wt % specimen and, then, a reduction in the elongation at break of 22.2 and 75.9% was observed for the samples incorporating 2 and 3 wt % CNW. In any case, owing to the great variability of data, concentrations lower than 3 wt % did not produce statistically significant improvements.

When incorporating freeze-dried CNW, the material became less ductile when compared with the 2% CNW FD-P sample due to the lower degree of dispersion and lower matrix–filler adhesion attained in the former one.

The material was significantly stiffer and more brittle when incorporating freeze-dried BCNW through the precipitation method than with CNW, suggesting that stronger filler–filler interactions are developed in the case of BCNW. On the other hand, no significant changes were observed for the direct melt-mixing of freeze-dried CNW and BCNW.

The elastic modulus experimental values versus the theoretical ones obtained by applying the Halpin–Tsai model are shown in Figure 8. For the nanocomposites incorporating CNW, with an experimental aspect ratio of ~12, the percolation threshold should lay around 6 vol % of CNW. In this figure, it is observed how the elastic modulus increases with the CNW loading, but even the maximum CNW loading tested, that is, 2.3 vol % is far below the percolation threshold, and thus it might be possible to further enhance the mechanical properties with higher nanofiller loadings. In the same way that with BCNW, the experimental values were found below the ones predicted by the model, which, in this case, may be explained by a combination of a certain degree of nanofiller agglomeration and to the fact that the loadings were below the percolation threshold.

Thermal Stability of the Different EVOH/Plant CNW Nanocomposite Films. Finally, the effect of the CNW's incorporation on the thermal stability of the nanocomposite films was evaluated by TGA. As observed for BCNW, the degree of dispersion of the nanofiller seemed to be related to the degradation profile, and thus, poorer dispersion of the filler led to broader degradation range.

Table V. Young's Modulus, Tensile Strength, and Elongation at Break for EVOH32 and EVOH Composites Incorporating BC and BCNW

	E (GPa)	Tensile strength (MPa)	E_b (%)	Toughness (J)
EVOH	^{a}1.37 ± 0.18	^{a}51.99 ± 4.96	^{a}93.35 ± 56.52	0.36 ± 0.14
1%CNW FD-P	^{a,b}1.41 ± 0.11	^{a}51.16 ± 2.73	^{a}98.67 ± 61.85	0.27 ± 0.18
2%CNW FD-P	^{a,b}1.51 ± 0.05	^{a}52.34 ± 1.74	^{a}72.67 ± 14.19	0.22 ± 0.04
3%CNW FD-P	^{b}1.65 ± 0.09	^{a}56.36 ± 4.66	^{a}22.50 ± 17.33	0.08 ± 0.04
2%CNW FD	^{a,b}1.54 ± 0.08	^{a}56.06 ± 3.19	^{a}13.50 ± 6.61	0.07 ± 0.04

The a and b letters correspond to the ANOVA statistical analysis and Tukey test of the data that indicate that with a 95% confidence level, and the values are significantly different.

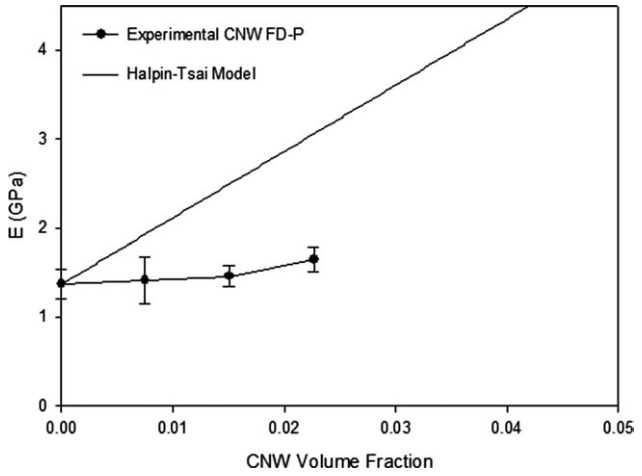

Figure 8. Experimentally measured Young's modulus for EVOH-CNW FD-P nanocomposites compared to theoretical predictions by Halpin–Tsai.

From Table VI, it can be observed that degradation temperatures tended to be slightly lower for CNW-loaded composites than for those containing BCNW, which is in agreement with the lower thermal stability of CNW previously assessed.[18] But again, these nanocomposites showed degradation profiles similar to the ones from neat EVOH and far above the processing window of EVOH materials.

CONCLUSIONS

In this work, EVOH/CNW composite films were produced by the melt compounding technique, and the effects of the cellulose source, nanofiller concentration, and pre-incorporation method in the crystallinity, water vapor permeability, mechanical properties, and thermal stability of the generated materials were investigated. The crystallinity index of the material was found to increase with improved dispersion and nanofiller loadings, and it was also higher for the more crystalline BCNW than for plant CNW. Water permeability was strongly influenced by the filler incorporation method. Therefore, while the agglomeration observed in the films directly incorporating freeze-dried BCNW was detrimental for the nanocomposite barrier properties, increasing the tortuosity of the diffusion pathway by incorporating fiber entanglements led to a reduction of ~67% for the 2% BC FD-P sample. However, even though the proposed preincorporation methods led to highly dispersed nanofillers, no significant improvements were observed in the water barrier properties of these materials, which could be explained by the increase in the amorphous density caused by the presence of the dispersed fillers, which counteracted the lower water sorption caused by the increase in the overall crystallinity generated.

The mechanical properties were related to the filler–filler and matrix–filler interactions, which were modified by the incorporation method. In this case, the nanofiller loading was an important parameter, because reaching the percolation threshold, which corresponded to 3% wt % BCNW, allowed the production of nanocomposites with increased elastic modulus and tensile strength but still maintaining a relatively ductile behavior.

Table VI. TGA Maximum of the Weight Loss First Derivate (T_D) and the Corresponding Peak Onset and Endset Values for the EVOH-Based Nanocomposites

	Onset T (°C)	T_D (°C)	Endset T (°C)
EVOH	268.9	398.7	483.6
1%CNW Precip	287.9	377.1	478.3
2%CNW Precip	303.3	395.8	475.1
3%CNW Precip	305.6	394.9	473.7
2%CNW FD	279.6	400.6	475.5

The incorporation of BCNW through electrospun fibers resulted in nanocomposites with a high dispersion level, but the selected loading was not optimal for the formation of the nanofiller percolation network. As a result, the material did not show any significant improvement on the mechanical and barrier properties. The traditional method of directly incorporating freeze-dried BCNW was also detrimental for the mechanical properties, as the prevalence of filler–filler interactions due to agglomeration and poor interfacial addition led to a rigid and fragile material. When incorporating plant CNW, the barrier and mechanical properties were not significantly modified, probably due to the fact that greater loadings are required for reaching the percolation threshold. Nevertheless, the incorporation of freeze-dried material seemed to favor the blocking capacity of CNW, which was also higher than for freeze-dried BCNW. Finally, the thermal stability of all the developed EVOH-based materials was high enough for melt processing and was not significantly reduced upon addition of the different cellulose fillers.

ACKNOWLEDGMENTS

M. Martínez-Sanz thanks the Spanish Ministry of Education for the FPU grant 1484. A. Lopez-Rubio is the recipient of a "Ramon y Cajal" contract from the Spanish Ministry of Science and Innovation. The authors acknowledge the financial support from MICINN (MAT2009-14533-C02-01 project). Roxane Penades, on leave from the U. of Grenoble in France, is acknowledged for her dedication and support in the experimental work related to plant cellulose nanowhiskers.

REFERENCES

1. Lagaron, J. M.; Powell, A. K.; Bonner, G. *Polym. Test.* **2001,** *20*, 569.
2. Lagaron, J. M.; Giménez, E.; Altava, B.; Del-Valle, V.; Gavara, R. *Macromol. Symp.* **2003,** *198*, 473.
3. López-Rubio, A.; Lagaron, J. M.; Giménez, E.; Cava, D.; Hernandez-Muñoz, P.; Yamamoto, T.; Gavara, R. *Macromolecules* **2003,** *36*, 9467.
4. Aktzi, N.; Nir, Y.; Wang, D.; Narkis, M.; Siegmann, A. *Polym. Compos.* **2001,** *22*, 710.
5. Franco-Urquiza, E.; Perez, J. G.; Sánchez-Soto, M.; Santana, O. O.; Maspoch, M. L. *Polym. Int.* **2010,** *59*, 778.
6. Cabedo, L.; Giménez, E.; Lagaron, J. M.; Gavara, R.; Saura, J. *J. Polymer* **2004,** *45*, 5233.

7. Fernández, A.; Sánchez, M. D.; Ankerfors, M.; Lagaron, J. M. *J. Appl. Polym. Sci.* **2008,** *109*, 126.
8. Sanchez-Garcia, M. D.; Lagaron, J. M. *Cellulose* **2010,** *17*, 987.
9. Sanchez-Garcia, M. D.; Hilliou, L.; Lagaron, J. M. *J. Agric. Food Chem.* **2010,** *58*, 12847.
10. Jiang, L.; Morelius, E.; Zhang, J.; Wolcott, M.; Holbery, J. *J. Compos. Mater.* **2008,** *42*, 2629.
11. Oksman, K.; Mathew, A. P.; Bondeson, D.; Kvien, I. *Compos. Sci. Technol.* **2006,** *66*, 2776.
12. Bondeson, D.; Oksman, K. *Compos., Part A: Appl. Sci. Manuf.* **2007,** *38*, 2486.
13. Rojas, O. J.; Montero, G. A.; Habibi, Y. *J. Appl. Polym. Sci.* **2009,** *113*, 927.
14. Peresin, M. S.; Habibi, Y.; Zoppe, J. O.; Pawlak, J. J.; Rojas, O. *J. Biomacromolecules* **2010,** *11*, 674.
15. Olsson, R. T.; Kraemer, R.; Lopez-Rubio, A.; Torres-Giner, S.; Ocio, M. J.; Lagaron, J. M. *Macromolecules* **2010,** *43*, 4201.
16. Martínez-Sanz, M.; Olsson, R. T.; Lopez-Rubio, A.; Lagaron, J. M. *Cellulose* **2011,** *18*, 335.
17. Martínez-Sanz, M.; Olsson, R.; Lopez-Rubio, A.; Lagaron, J. *J. Appl. Polym. Sci.* **2012,** *124*, 1398.
18. Martínez-Sanz, M. L.-R., A.; Lagaron, J. *J. Appl. Polym. Sci.*, **2012**, DOI: 10.1002/app.38433.
19. Wang, N.; Ding, E.; Cheng, R. *Polymer* **2007,** *48*, 3486.
20. O′Sullivan, A. C. *Cellulose* **1997,** *4*, 173.
21. Moharram, M. A.; Mahmoud, O. M. *J. Appl. Polym. Sci.* **2007,** *105*, 2978.
22. Belbekhouche, S.; Bras, J.; Siqueira, G.; Chappey, C.; Lebrun, L.; Khelifi, B.; Marais, S.; Dufresne, A. *Carbohydr. Polym.* **2011,** *83*, 1740.
23. Sanchez-Garcia, M. D.; Gimenez, E.; Lagaron, J. M. *Carbohydr. Polym.* **2008,** *71*, 235.
24. Maxwell, J. C. A Treatise on Electricity and Magnetism. Clarendon Press, Oxford, UK, Vol. *1*; **1881;** pp 435–449.
25. Fricke, H. *Phys. Rev.* **1924,** *24*, 575.
26. Paul, D. R.; Bucknall, C. B. Polymer Blends, Vol. *2*: Performance. Wiley InterScience: New York, **2000.**
27. Luo, J. J.; Daniel, I. M. *Compos. Sci. Technol.* **2003,** *63*, 1607.
28. Sanchez-Garcia, M. D.; Lagaron, J. M. *J. Appl. Polym. Sci.* **2010,** *118*, 188.
29. George, J.; Ramana, K. V.; Bawa, A. S.; Siddaramaiah, S. *Int. J. Biol. Macromol.* **2011,** *48*, 50.
30. Mirzataheri, M.; Atai, M.; Mahdavian, A. R. *J. Appl. Polym. Sci.* **2010,** *118*, 3284.
31. Siqueira, G.; Bras, J.; Dufresne, A. *Biomacromolecules* **2009,** *10*, 425.
32. Petersson, L.; Oksman, K. *Compos. Sci. Technol.* **2006,** *66*, 2187.
33. Tashiro, K.; Kobayashi, M. *Polymer* **1991,** *32*, 1516.
34. Hajji, P.; Cavaille, J. Y.; Favier, V.; Gauthier, C.; Vigier, G. *Polym. Compos.* **1996,** *17*, 612.